there must be also be a part of the rotation (off-)axis velocity pattern that does not depend on time.

23. B. Romanowicz, X.-D. Li, J. Durek, *Science* **274**, 963 (1996).
24. Song and Richards (*2*) relied on high-quality observations, but these were relatively few in number and they investigated only three source-receiver paths to obtain the time variations. In comparison, we used noisier ISC data, but because each CAS value was derived on average from 230 observations, the standard error of the mean should be ~0.1 s. The spatial uniformity of the CAS averages in Fig. 3 testifies to their accuracy. Because of the dense data coverage, we can simultaneously determine both the spatial and temporal variations of the residuals, inverting for both the magnitude and orientation of the anisotropy as a function of time. The analysis in (*2*) required Song and Richards to assume both the geometry (constant model of anisotropy and tilt of the symmetry axis) and process (rigid rotation about an axis coinciding with the mantle rotation axis) to interpret their observations. Still, data for the second path (Kermadec to Kongsberg) give time variations inconsistent with the model. The factor of 3 difference between the rotation rates obtained in (*2*) and in the present study is at least partly attributable to the model of anisotropy used by Song and Richards for the inner core. The magnitude of anisotropy they assumed is about twice that of model IAC4B (*14*), for example, and had they used this model, they would have obtained a rotation rate of ~2° year^{-1}. We inverted for the magnitude of anisotropy in the present study.
25. The time-dependent solution (Fig. 4C) is dominated by the harmonics Y_2^1 and Y_4^1, whose sum has a maximum at ~60°N. Thus, observations at corresponding values of the angle ζ, the angle that a ray forms with the axis of symmetry, should be the best for monitoring the rotation of the inner core. This is confirmed in Fig. 4D, which shows the time derivative of Fig. 4C (the relatively large effects predicted for low latitudes may be contaminated by noise, because the CAS coverage below 30° has had large gaps during the early time intervals; Fig. 2). The predicted solutions for the earliest and latest time periods compare well with the data (Fig. 4, E and F) as well as with the spherical-harmonic expansion for the same time periods (Fig. 2, A and F).
26. K. Lambeck, *The Earth's Variable Rotation: Geophysical Causes and Consequences* (Cambridge Univ. Press, New York, 1980); *Geophysical Geodesy: The Slow Deformations of the Earth* (Oxford Univ. Press, New York, 1988).
27. This angular acceleration value, -5×10^{-22} rad s^{-2}, is an average for the past 2 millennia and has varied by <50% over this time period (*26*). Because of the need for a large backward extrapolation in time, however, its uncertainty for the present application is difficult to evaluate.
28. A naïve analysis would attempt to relate the lag time $\tau = 10^5$ years (3×10^{12} s) between the inner core and mantle with the viscous coupling time $t_\nu = d^2/\nu$, where d is the thickness (2.25×10^6 m) and ν is the kinematic viscosity of the outer core. The result, $\nu \sim 2$ m^2 s^{-1} [viscosity $\eta = \nu\rho \sim 2 \times 10^4$ Pa·s, using a density of $\rho = 1.1 \times 10^4$ kg m^{-3}; A. M. Dziewonski and D. L. Anderson, *Phys. Earth Planet. Inter.* **25**, 297 (1981)], is orders of magnitude greater than current estimates for the viscosity of the outer core (*37–39*). This approach, however, disregards the essentially two-dimensional character of rotating flows (as expressed by the Taylor-Proudman theorem); momentum need only be transmitted across a thin (Ekman) boundary layer rather than the full thickness of the fluid layer (*29, 40, 41*). The characteristic time for momentum transfer is thereby shortened by a factor of $E^{1/2}$, where the Ekman number $E = \nu/d^2\Omega \sim 3 \times 10^{-16}$, yielding a rotation rate $\Omega = 7.3 \times 10^{-5}$ rad s^{-1} (compare D. L. Book and J. A. Valdivia, *J. Plasma Phys.*, in press).
29. D. Gubbins and P. H. Roberts, in *Geomagnetism*, J. A. Jacobs, Ed. (Academic Press, Orlando, FL, 1987), vol. 2, pp. 1–23.
30. Equating the lag time $\tau \approx 10^5$ years (3×10^{12} s) with the "spin-up" time $t_E = d/(\nu\Omega)^{1/2}$, where d is the thickness of the outer core and Ω is Earth's rotation rate, yields a value for the kinematic viscosity $\nu \sim 10^{-8}$ m^2 s^{-1} for the outer-core fluid [viscosity $\eta = \nu\rho \sim 10^{-4}$ Pa·s (*29, 40–42*)]. Taking into account the Lorentz forces associated with the magnetic field leads to a magnetic spin-up time $\tau_M = \tau_E/(\alpha\sqrt{2})$ in the case of strong fields ($\alpha > 2$) (*42*). Here, the magnetic interaction parameter or Elsasser number, $\alpha^2 = B^2\sigma/(2\rho\Omega) \approx 3.7 \times 10^5 B^2$ in SI units (where B is the magnetic field) gives the ratio of Lorentz to Coriolis forces (*20, 29*) [the electrical conductivity of the outer-core fluid, $\sigma = 6\ (\pm 3) \times 10^5$ S m^{-1}, is relatively well known from high-pressure experiments (*38*)]. Because the total strength of the magnetic field deep inside the core is not well known, the magnitude of the Elsasser number α^2 is also uncertain. Downward extrapolation of the present-day field observed at Earth's surface yields a value of $B \sim 10^{-3}$ T for the radial inductance at the base of the mantle, but it is known that this is only part of the field existing deep inside the core; various theoretical estimates bound the characteristic value of the field inside the core between $\sim 10^{-1}$ and 10^{-4} T (*20, 29, 31*). The Elsasser number is therefore within the range $\sim 10^{-3}$ to 10^3 (*20, 29*). For the "weak-field" case, which uses the "observed" value $B \sim 10^{-3}$ T, $\alpha^2 \sim 0.4$. If we equate τ_M with the lag time $\tau \approx 10^5$ years identified above for the inner-core rotation, we obtain a value $\nu B^2 \approx 10^{-14}$ T^2 m^2 s^{-1} for the product of kinematic viscosity and squared magnetic field in the outer core. Using the observed magnetic field at the bottom of the mantle (weak-field value $B \sim 10^{-3}$ T) again yields a low value of viscosity, $\nu \sim 10^{-8}$ m^2 s^{-1}, for the outer-core fluid. Indeed, values of kinematic viscosity above the range 10^{-7} to 10^{-6} m^2 s^{-1} imply unacceptably small values for the magnetic field in the core (*20, 29, 31*).
31. G. A. Glatzmaier and P. H. Roberts, *Nature* **377**, 203 (1995); *Phys. Earth Planet. Inter.* **91**, 63 (1995).
32. D. Gubbins, *J. Geophys. Res.* **86**, 11695 (1981).
33. In the Glatzmaier-Roberts model (*31*), the eastward rotation of the inner core relative to the mantle is maintained by magnetic coupling between the solid inner core and the fluid just above it, which is flowing eastward because of a thermal-wind effect (G. A. Glatzmaier, personal communication). As in their original simulation, their latest results show an eastward rotation of the inner core that varies in magnitude between 2° and 3° year^{-1} relative to the mantle.
34. S. R. C. Malin and B. M. Hodder, *Nature* **296**, 726 (1982); M. G. McLeod, *J. Geophys. Res.* **90**, 4597 (1985).
35. The magnetic diffusivity of the core metal, $\eta_m = (\mu_0\sigma)^{-1} \approx 1$ m^2 s^{-1} (where μ_0 is the magnetic permeability of free space and σ is the elastical conductivity of the outer-core fluid), is sufficiently high that field lines diffuse $\sim 6 \times 10^4$ m into the inner core within a century (*20, 29, 38*); see also R. Hollerbach and C. A. Jones, *Nature* **365**, 541 (1993).
36. Scaling analysis between the core and atmosphere shows that a few years' seismological monitoring of the inner-core motion corresponds to hourly observations of the weather.
37. C. R. Gwinn, T. A. Herring, I. I. Shapiro, *J. Geophys. Res.* **91**, 4755 (1986).
38. R. Jeanloz, *Annu. Rev. Earth Planet. Sci.* **18**, 357 (1990).
39. E. Wasserman, L. Stixrude, R. E. Cohen, *Eos* **77**, S268 (1996).
40. H. Bondi and R. A. Lyttleton, *Proc. Camb. Philos. Soc.* **44**, 345 (1948).
41. H. P. Greenspan, *The Theory of Rotating Fluids* (Cambridge Univ. Press, New York, 1968).
42. E. R. Benton and A. Clark Jr., *Annu. Rev. Fluid Mech.* **6**, 257 (1974); see also D. E. Loper, *Phys. Fluids* **13**, 2995 (1970); R. G. Davis, *Geophys. Res. Lett.* **21**, 1815 (1994).
43. We thank G. Glatzmaier, D. Loper, M. Manga, P. Olson, P. H. Roberts, B. Romanowicz, L. Stixrude, J. Tromp, and G. Ekström for helpful discussions, as well as X.-D. Song and P. G. Richards for sending us a copy of their paper before publication and for subsequent discussions. This work was initiated while A.M.D. was a visiting professor in the Miller Institute for Basic Research in Science (March 1995) and was supported by NSF and NASA.

12 June 1996; accepted 20 September 1996

Rotation and Magnetism of Earth's Inner Core

Gary A. Glatzmaier* and Paul H. Roberts

Three-dimensional numerical simulations of the geodynamo suggest that a super-rotation of Earth's solid inner core relative to the mantle is maintained by magnetic coupling between the inner core and an eastward thermal wind in the fluid outer core. This mechanism, which is analogous to a synchronous motor, also plays a fundamental role in the generation of Earth's magnetic field.

Three-dimensional (3D) numerical simulations of the geodynamo, the mechanism in Earth's core that generates the geomagnetic field, showed that a magnetic field with an intensity, structure, and time dependence similar to that of Earth's can be maintained by a convective model (*1, 2*). The convection, which takes place in the fluid outer core surrounding the solid inner core, twists and shears magnetic field, continually generating new magnetic field to replace that which diffuses away. The model we describe here (*2*) assumes the mass, dimensions, and basic rotation rate of Earth's core, an estimate of the heat flow out of the core, and, as far as possible, realistic material properties (*3*).

Convection is driven by thermal and compositional buoyancy sources that develop at the inner core boundary as the Earth cools and iron alloy solidifies onto the inner core (*4*). For simplicity, we modeled the core as a binary alloy (*5*). Our boundary conditions at the inner core boundary constrain the local fluxes of the latent heat and

G. A. Glatzmaier, Institute of Geophysics and Planetary Physics, Los Alamos National Laboratory, Los Alamos, NM 87545, USA. E-mail: gag@lanl.gov
P. H. Roberts, Institute of Geophysics and Planetary Physics, University of California, Los Angeles, CA 90095, USA. E-mail: roberts@math.ucla.edu

*To whom correspondence should be addressed.

the light constituent to be proportional to each other and to the local cooling rate. The flux of the light constituent provides three times as much buoyancy as the latent heat flux. However, the vigor of the convection, the strength of the magnetic field, and the angular velocity of the inner core are all ultimately determined by the thermal boundary condition at the core-mantle boundary. We prescribed a heat flow through it of 7.2 TW, which is geophysically realistic (6), 5.0 TW of this being the heat conducted down the adiabatic part of the temperature gradient.

The inner core in our model is free to rotate about the geographic axis in response to the magnetic and viscous torques to which the outer core subjects it (7). We found that the inner core rotates relative to the mantle in the eastward direction, at an angular velocity of $\Omega_{IC} \sim 2°$ to $3°$ per year (8). Our prediction of eastward inner core rotation is consistent with two subsequent, independent analyses of seismic data: Song and Richards (9) first estimated $\Omega_{IC} \sim 1°$ per year, and then Su *et al.* (10) estimated $\Omega_{IC} \sim 3°$ per year. Considering the uncertainties in our model and material properties and in the seismic data and inner core anisotropy, these preliminary theoretical and observational results are in reasonable agreement.

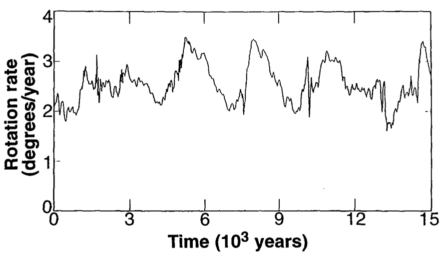

Fig. 1. Eastward angular velocity of the inner core relative to the mantle for the last 15,000 years of our simulation.

For a typical 15,000-year interval, our mean Ω_{IC} is $\overline{\Omega}_{IC} \approx 2.6°$ per year (Fig. 1). The standard deviation about that mean is 0.4°/year, the root mean square of $\dot{\Omega}_{IC}$ is $\dot{\Omega}_{IC}^{\,rms} = 0.005°$ per year^2, and the time scale of variations of Ω_{IC} is $\tau_{IC} = \overline{\Omega}_{IC}/\dot{\Omega}_{IC}^{\,rms} \approx 500$ years. However, there is also a distinct 3000-year period with an amplitude variation of about a $\pm 0.5°$ per year (Fig. 1).

To explain the sense of rotation of the inner core relative to the mantle, it is helpful to recognize that the inner core plays a central role in the dynamics of the outer core (11). Consider an imaginary circular cylinder coaxial with the rotation axis and touching the inner core at its equator. This "tangent cylinder" divides the outer core into an interior region I and an exterior region E. The interior region consists of a northern polar region I_N and a southern polar region I_S.

Convection in a rapidly rotating body of fluid, like Earth's outer core, takes the form of Taylor columns, which have axes parallel to the rotation axis (12) and fluid flowing in planes perpendicular to it. However, when the fluid flow generates a strong magnetic field that in turn feeds back onto the flow by means of Lorentz forces, the flow structure is somewhat different. In our simulation (2), several nonaxisymmetric magnetically suppressed Taylor columns exist in E, whereas in I, although the flow is also mainly in planes perpendicular to the rotation axis, it is nearly axisymmetric and sheared parallel to the rotation axis. Consequently, heat and light elements are more efficiently transported from the inner core boundary to the core-mantle boundary by the nonaxisymmetric flows in E than by the nearly axisymmetric flow in I, which takes a more indirect, helical route to the core-mantle boundary. As a result, in our simulation (2) the axisymmetric parts of the perturbations of the entropy and light constituent (relative to their constant basic-state values) at a given radius near the inner core boundary are roughly five times greater in I than their respective values in E. The associated buoyancy force in I produces an outward flow along the rotation axis, which (because of mass conservation) requires a flow directed toward the rotation axis near the inner core boundary and away from the axis near the core-mantle boundary. This axisymmetric part of the flow is called the meridional circulation (Fig. 2A). Because the angular momentum of fluid parcels is approximately conserved, fluid flowing toward the rotation axis just outside of the inner core boundary, in I_N and I_S, is spun up; fluid flowing away from the axis near the core-mantle boundary is spun down. The resulting zonal flow in I is eastward near the inner core and westward near the mantle, relative to the fluid in E and to the mantle (Fig. 2B). In atmospheric contexts, these

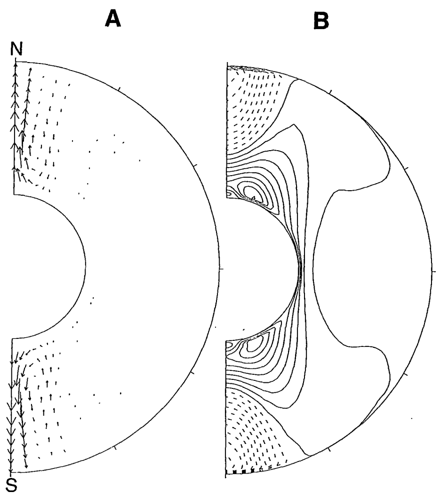

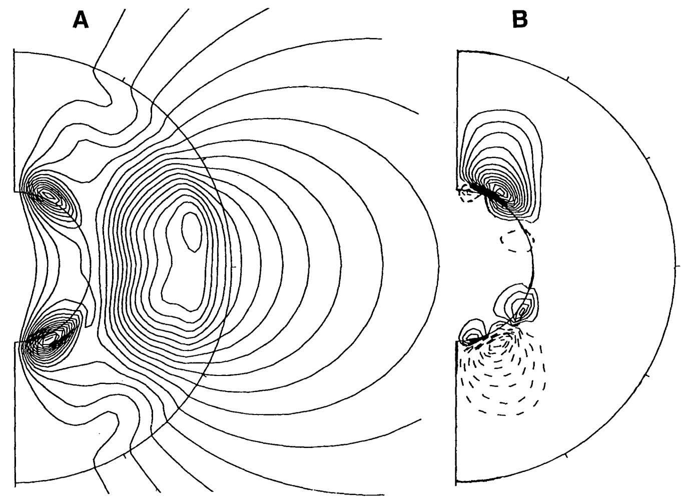

Fig. 2 (**left**). Snapshots in the meridian plane of (**A**) the axisymmetric meridional fluid flow and (**B**) the axisymmetric zonal fluid flow. The direction of the arrows in (A) are parallel to the flow; their length is proportional to the flow speed. Contours of constant angular velocity ω are shown in (B); solid lines correspond to eastward flow relative to the mantle, and dashed lines, to westward flow. The maximum meridional flow in (A) is 6×10^{-4} m/s; the maximum angular velocity in (B) is 5° per year (contour interval is 0.5° per year). Of particular interest is the contour line adjacent to the inner core boundary, which indicates that the inner core is moving eastward. Note also that the equatorial region of the outer core has a weak westward angular velocity, which helps to conserve total angular momentum of our model Earth and is partially responsible for the typical 0.2° per year westward drift that our magnetic field displays at the core-mantle boundary. **Fig. 3** (**right**). Snapshots in the meridian plane of (**A**) the axisymmetric meridional magnetic field and (**B**) the axisymmetric zonal magnetic field. The magnetic lines of force are counterclockwise in (A), and the maximum magnetic intensity is about 25 mT. The contours in (B) are solid for eastward-directed magnetic field and dashed for westward-directed field; the maximum magnetic intensity is about 13 mT (1-mT contour intervals). Of particular interest is the expulsion of zonal field from much of the inner core.

zonal jets would be described as part of a "thermal wind" (*13*), but because strong magnetic fields also exist in the core, especially inside the tangent cylinder, the term "thermal wind" is not precisely correct. However, the strong zonal (east-west) fields (Figs. 3B and 4) are not affected by the zonal velocity because there is little motion across those field lines. The differential zonal flow does shear the strong north-south (meridional) fields (Figs. 3A and 4), but the concentration of these fields along the rotation axis minimizes this effect.

In assessing the effect of these eastward jets on the motion of the inner core, it is helpful to have two physical pictures in mind. The first is based on Alfvén's theorem, which states that magnetic lines of force move with a perfectly conducting medium as though frozen to it. The core is not a perfect electrical conductor, so this theorem does not apply precisely to Earth. Nevertheless, it provides a qualitative description of electromagnetic induction in a moving fluid, in terms of which lines of force passing through the jets tend to be carried eastward with the fluid. These lines of force permeate the inner core (Figs. 3A and 4), and if there is relative motion between the inner core and the jets, the lines of force will lengthen, according to Alfvén's theorem.

The second physical picture describes the dynamical effects of a magnetic field **B** in terms of Faraday-Maxwell stresses, in which magnetic lines of force are in a state of tension. Any relative angular displacement that lengthens the lines of force linking the solid inner core to the fluid outer core above it is resisted by that tension; so, on average, the inner core corotates with the fluid above it. This mechanism has an analogy in electrical engineering: the synchronous motor, where the inner core represents the rotor of an electric motor that is locked synchronously to the eastward propagating magnetic field at the base of the fluid core, created by the convective dynamo operating above it (*1, 2*).

The "corotation" between the inner core and the fluid lying just above it (*14*) is a generalized view. At any given time, the solid inner core has only one angular velocity, Ω_{IC}, but the angular velocity ω of the fluid jets is a function of position. By corotation we mean that the inner core is rotating at some weighted average of the eastward fluid flow above it such that the net torque on the inner core about the rotation axis is nearly zero. Because the peak zonal flow occurs near the rotation axis, the inner core usually rotates more slowly than the fluid above it in the polar regions and faster than the fluid above it in the equatorial region (Fig. 2B). On areas of the inner core surface where $B_rB_\phi > 0$, the tension of the magnetic field lines increases the eastward Ω_{IC}; where $B_rB_\phi < 0$, it decreases it (*7*). Consider the longitudinally averaged field structure in the snapshot of Fig. 3. The outward-directed field B_r at mid- and high latitude in the northern hemisphere (Fig. 3A) is sheared into eastward-directed field B_ϕ (Fig. 3B); the opposite occurs in the southern hemisphere. However, in both places the product $B_rB_\phi > 0$, which exerts a local, eastward magnetic stress on the inner core. Therefore, the fluid flow and magnetic coupling at the inner core boundary are fundamental to both the rotation of the inner core and the generation of the magnetic field in the outer core.

Magnetic field is also generated by the differential zonal flows (Fig. 2B) in I_N and I_S that shear the meridional fields (Fig. 3A) into zonal fields (Fig. 3B). This field generation maintains a helical magnetic field inside the tangent cylinder (Fig. 4), a combination of the strong meridional field near the rotation axis and the strong zonal field near the tangent cylinder. Recall that the flow is also mainly meridional near the rotation axis and zonal near the tangent cylinder in order to minimize distortion of the field. Our dynamically consistent simulations (*1, 2*) suggest that the geodynamo develops 3D flow and field structures that produce a delicate, nonlinear balance between the generation of new field by flow structures that twist and shear it and the avoidance of too much resistance to the flow by field structures that are almost force-free in places.

The difference in the structure of the magnetic field between the inner core and the outer core (Fig. 4) may be understood in the following way: The electromagnetic time constant τ_{em} of the inner core is of the order of 10^3 years (*15*), so magnetic fields in the outer core that vary on the time scale of the convection (10^2 years) cannot penetrate far into the inner core. In particular, the time-dependent asymmetric fields, even those of large spatial scale, do not penetrate deeply. However, slowly varying axisymmetric fields, such as those associated with the axial dipole of the Earth, have time to penetrate the inner core completely (Figs. 3A and 4). Because of ohmic dissipation, the associated electric currents deep within the inner core are almost zero, so these slowly varying axisymmetric magnetic fields are good approximations of "potential fields." Zonal fields generated by the global departure of ω from Ω_{IC} do not penetrate far into the inner core because the time scale for reestablishing corotation is very short, and zonal fields created by local departures of ω from Ω_{IC} do not penetrate far into the inner core because of their small spatial scales (Fig. 3B). Therefore, the only fields that persist deep in the inner core are the nearly axisymmetric, potential-like fields, which are nearly parallel to the rotation axis (Fig. 4). These are the fields that provide the magnetic coupling between the inner and outer cores. However, although their maximum strength at the inner core boundary can be as high as 10 mT, they are concentrated in the polar regions (Fig. 4) and so have small moment arms. Therefore, the restoring torques that maintain corotation are not as large as they would otherwise be.

This explanation of why a time-averaged eastward $\overline{\Omega}_{IC}$ is required to bring about a statistically steady state in which

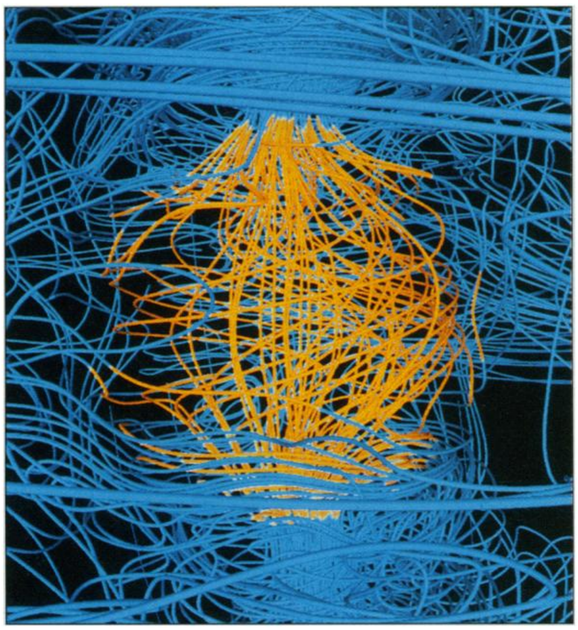

Fig. 4. Snapshot of magnetic lines of force in the core of our simulated Earth. Lines are gold (blue) where they are inside (outside) of the inner core. The axis of rotation is vertical in this image. The field is directed inward at the inner core north pole (top) and outward at the south pole (bottom); the maximum magnetic intensity is about 30 mT.

the time average of the magnetic torque on the inner core $\overline{\Gamma}_B$ is zero ignores the time-average of the viscous torque $\overline{\Gamma}_\nu$ on the inner core (*7*). With a nonzero fluid viscosity, $\overline{\Omega}_{IC}$ adjusts itself so that $\overline{\Gamma}_B + \overline{\Gamma}_\nu = 0$, implying that, because $\overline{\Gamma}_B$ drags the inner core eastward, $\overline{\Gamma}_\nu$ must be acting westward. However, even though the fluid viscosity in our models (*1, 2*) is several orders of magnitude greater than is likely for the real Earth, the viscous torque on the inner core has little effect.

To demonstrate its effect, we replace our no-slip condition on the zonal flow at the inner core boundary by a viscous stress-free condition, which makes $\Gamma_\nu = 0$, and then continue the integration (*16*). The contours of constant ω near the inner core no longer resemble those in Fig. 2B but, instead, all intersect the inner core boundary. Apart from this, the solution strongly resembles the original one (*2*). The mean Ω_{IC} is still eastward, and the magnitude of Γ_B about its zero time-average is on the order of 10^{16} N m. This value is small enough that Ω_{IC} remains relatively constant on a time scale of decades. It is also small in the sense that the large local magnetic stresses nearly cancel out when integrated over the inner core boundary. That is, when we integrate the absolute value of the moment of the magnetic stress $|B_r B_\phi|/\mu_0$ [instead of $B_r B_\phi/\mu_0$ (*7*)] over the inner core boundary, we consistently obtain values three orders of magnitude greater than Γ_B.

In a further experiment, still using the viscous stress-free boundary condition, we instantaneously reset Ω_{IC} to zero and continue the integration (Fig. 5). As the radial field becomes sheared by the differential motion, the restoring magnetic torque quickly increases, attaining a maximum of 6×10^{18} N m within a couple months. After about 2 years, corotation is completely reestablished (Fig. 5), and the magnitude of Γ_B is again on the order of 10^{16} N m with a zero mean value.

This simple test illustrates the "synchronous motor" mechanism and how short a time is required to spin up Earth's inner core by magnetic torque alone compared with its viscous spin-up time (~10^4 years). This 2-year magnetic spin-up time is also short compared with the magnetic diffusion time for the inner core, $\tau_{em} \sim 10^3$ years (*15*). Another way to look at this is to realize that more than 99% of the energy of the magnetic field is inside the core (10% in the inner core) (*1, 2*), which is typically 10,000 times more energy than the kinetic energy of the rotation of the inner core relative to the mantle. In addition, our simulation predicted a time-dependent Ω_{IC} (Fig. 1) in rough agreement with recent seismic analyses (*9, 10*) without our model Earth spinning down; that is, we neglected the lunar tidal forces on Earth and instead constrained the total angular momentum of our inner core, outer core, and mantle to be constant (*7*).

Earth's angular momentum is, however, slowly decreasing because of tidal forces; it has been suggested (*10*) that the superrotation of the inner core may be the result of a viscous time lag relative to the spin down of the mantle. However, this explanation relies only on the small viscous torques at the boundaries of the fluid core and ignores the much larger effects of rotating convection and magnetic coupling. For the reasons stated above, we feel that the synchronous motor mechanism plays a much greater role in determining the superrotation of Earth's inner core than would a viscous time-lag mechanism. Also, unlike the viscous time-lag mechanism, which implies a monotonically decreasing inner core rotation rate, our mechanism (Fig. 1) suggests that Earth's inner core has spun both faster and more slowly at times in the past than it is spinning today and predicts that it will spin both faster and more slowly in the future according to the evolving magnetohydrodynamics of Earth's fluid core.

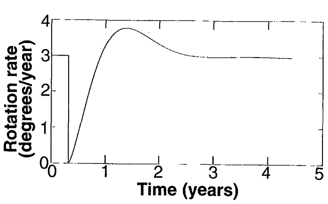

Fig. 5. Eastward angular velocity of the inner core relative to the mantle during the last 5 years of a test run for which no viscous torque was acting on the inner core. After instantaneously setting Ω_{IC} to zero, the magnetic torque reestablishes corotation within about 2 years.

REFERENCES AND NOTES

1. In our original geodynamo simulation [G. A. Glatzmaier and P. H. Roberts, *Phys. Earth Planet. Inter.* **91**, 63 (1995); *Nature* **377**, 203 (1995)], the core was assumed to be nearly uniform in density and temperature; buoyancy was included in the Boussinesq approximation.
2. Here we discuss the results of our most recent geodynamo simulation [G. A. Glatzmaier and P. H. Roberts, *Physica D* **97**, 81 (1996)], which included thermal and compositional convection in the core within the anelastic approximation.
3. The basic state of our iron-rich fluid core (relative to which the 3D time-dependent perturbations are solved) is hydrostatic and well mixed chemically and thermally, and has a spherically symmetric density profile fitted to the Preliminary Reference Earth Model (PREM) [A. M. Dziewonski and D. L. Anderson, *Phys. Earth Planet. Inter.* **25**, 297 (1981)]. We assumed no radioactive heating in the core (*17*) and that the electrical conductivities σ of the inner and outer cores are the same: 4×10^5 S/m. The eddy viscosity in our simulations (*1, 2*) is, from computational necessity, about three orders of magnitude larger than what would be expected for small-scale turbulence in Earth's fluid core and many orders of magnitude larger than its molecular viscosity. However, the viscous forces in the bulk of our fluid core are still about five orders of magnitude smaller than the Coriolis and Lorentz forces.
4. Because the melting temperature of core material increases with pressure more rapidly than does the temperature along the adiabat, the core presents the unfamiliar situation of a system that is cooled from the top but freezes from the bottom [J. A. Jacobs, *Nature* **172**, 297 (1953)].
5. For example, see S. I. Braginsky and P. H. Roberts, *Geophys. Astrophys. Fluid Dyn.* **79**, 1 (1995).
6. The rate of heat flow out of Earth's core is poorly known. Global 3D mantle convection simulations [P. J. Tackley, D. J. Stevenson, G. A. Glatzmaier, G. Schubert, *J. Geophys. Res.* **99**, 15877 (1994)] obtained 7.2 TW, the value we use. Stacey (*17*) estimates it to be 3.0 TW on the basis of the assumption that the age of the inner core is the same as the age of the Earth and that the rate of heat flow out of the core has remained constant during this time. However, we find in our (unpublished) simulations that a 3.0-TW boundary condition does not maintain a strong, Earth-like magnetic field. Because our 7.2-TW boundary condition (*2*) does maintain an Earth-like field, the age of Earth's inner core may be considerably less than the age of the Earth itself. Of course, many of the material properties that we assume are quite uncertain. For example, we assume that the mass of the light constituent released when a unit mass of alloy freezes at the inner core boundary is 0.065, and the corresponding entropy released is 190 J/(kg K); these have uncertainties of 10 and 50%, respectively (*5*). More significantly, the presence of radioactivity in the core would provide additional thermal buoyancy and therefore would require less compositional buoyancy to obtain similar convective vigor and magnetic field intensity with the same heat flow through the core-mantle boundary but without such a rapid growth rate of the inner core.
7. To obtain the angular velocity Ω_{IC}, we integrated the equation $C(d\Omega_{IC}/dt) = \Gamma_\nu + \Gamma_B$, where $C = 5.86 \times 10^{34}$ kg m^2 is the polar moment of inertia of the inner core and

$$\Gamma_\nu = \oint_{ICB} \bar{\rho}\bar{\nu} \frac{\partial \omega}{\partial r} r^2 \sin^2\theta dS$$

$$\Gamma_B = \frac{1}{\mu_0} \oint_{ICB} B_r B_\phi r^2 \sin\theta dS$$

are the viscous and magnetic torques on the inner core about the polar axis. Here, $\bar{\rho}$ and $\bar{\nu}$ are the fluid density and eddy viscosity in the basic state and μ_0 is the magnetic permeability; **B**, the magnetic field, and **V**, the fluid velocity (including the angular velocity ω), are obtained by integrating the magnetoconvective equations in the fluid core. The integrals defining Γ_ν and Γ_B are over the inner core boundary (ICB), and $dS = r^2 \sin\theta d\theta d\phi$ is an element of surface area. A similar equation of motion can be integrated for the angular velocity of the mantle Ω_M. However, because we apply no torque at the outer boundary of the mantle (that is, at the surface of our model Earth), the total angular momentum of our inner core, outer core, and mantle must remain constant; so we choose to constrain the total angular momentum to be exactly conserved each time step instead of applying the prognostic equation for Ω_M. All of our equations are actually solved in the rotating reference frame for which the total angular momentum of the inner core, outer core, and mantle is zero; therefore, the angular velocity of the inner core relative to the mantle, plotted in Fig. 1, is $\Omega_{IC} - \Omega_M$. However, Ω_M is typically more than two orders of magnitude smaller than Ω_{IC}.
8. This prediction was made as a result of our original geodynamo simulation (*1*). The amplitude of the eastward rotation of the inner core (relative to the mantle) was not substantially different from that derived from the model described here (*2*), although it fluctuated more strongly in time and was actually briefly westward during the polarity reversal

that that model executed during the simulation. The field threading the inner core was at that time very weak, so that the magnetic torque Γ_B was small. Note also that our models (*1, 2*) have assumed phase equilibrium on the inner core boundary; that is, as thermodynamic conditions change, freezing and melting occurs instantaneously to maintain the boundary at the freezing point. No allowance has been made for a finite time of relaxation to such a state. If that relaxation time were long compared with the time scales of interest in our model, the inner core would behave as a solid. As B. A. Buffett [*Geophys. Res. Lett.* **23**, 2279 (1996)] noted, the orientation of the inner core would then plausibly be gravitationally "locked" to that of the mantle by the inner core topography created by mantle inhomogeneities, which we have not included in our models. If Earth's inner core is rotating faster than the mantle, as recent observations suggest (*9, 10*), a short melting-freezing relaxation time, a "mushy zone" at the top of the inner core (D. E. Loper, private communication), or a low inner core viscosity (B. A. Buffett, private communication) may preclude this gravitational locking effect.

9. X. Song and P. G. Richards, *Nature* **382**, 221 (1996).
10. W. Su, A. M. Dziewonski, R. Jeanloz, *Science* **274**, 1883 (1996).
11. R. Hollerbach and C. A. Jones, *Nature* **365**, 541(1993); *Phys. Earth Planet. Inter.* **87**, 171 (1993).
12. For example, P. H. Roberts [*Philos. Trans. R. Soc. London Ser. A* **263**, 93 (1968)] analyzed convection in a sphere, rapidly rotating as measured by the Taylor number *Ta*. He showed that the critical temperature gradient, as measured by a Rayleigh number *Ra*, at which convection could marginally occur is of order $Ta^{2/3}$ for both axisymmetric and nonaxisymmetric modes of convection, but that the nonaxisymmetric motions, later identified by F. H. Busse [*J. Fluid Mech.* **44**, 441 (1970)] as rolls parallel to the rotation axis, have the smaller critical *Ra*. That such rolls are "preferred" can be qualitatively understood in terms of the Proudman-Taylor theorem: Slow, steady motions in an inviscid rotating fluid are 2D with respect to the rotation axis, so that a towed body in such conditions carries a column of fluid with it, a so-called Taylor column. The convective rolls are also often called, a little imprecisely, Taylor columns.
13. Similar thermal wind and meridional circulation structures were obtained by P. Olson and G. A. Glatzmaier [*Phys. Earth Planet. Inter.* **92**, 109 (1995)] using a fully 3D magnetoconvection model but with an imposed zonal magnetic field and a nonrotating, insulating inner core. Similar flow structures also have been obtained by C. Jones and R. Hollerbach (private communication) with their dynamo model using only one nonaxisymmetric mode.
14. Phrases like "just above the inner core boundary" are used in this discussion for presentational simplicity. The fluid in contact with the inner core boundary moves with it because of the no-slip boundary condition; there is no relative motion at the boundary. More precisely, the key quantities determining the coupling between inner and outer cores are B_r and the derivatives of **V** on the inner core boundary, which control B_ϕ and hence the stress $B_r B_\phi/\mu_0$ on the inner core boundary. Also, after writing this report we were given a preprint by J. Aurnou, D. Brito, and P. Olson (*Geophys. Res. Lett.*, in press) that describes a simple, analytic model of inner core rotation that approximates the thermal wind and magnetic coupling present in our geodynamo simulations (*1, 2*).
15. There is no generally accepted way of defining τ_{em}. We take $\tau_{em} = \mu_0 \sigma R^2/\pi^2$, where R is the Earth's inner core radius, which is appropriate for a sphere surrounded by an insulator. This gives $\tau_{em} \approx 2400$ years, which is large compared with typical time scales of the fluid motion. The magnetic fields emerging from the inner core impose time scales of order τ_{em} on the geodynamo mechanism and stabilize it against polarity reversals, a significant fact first suggested by Hollerbach and Jones (*11*) and confirmed by our simulations (*1, 2*). The absence of zonal field in an inner core coupled magnetically to a fluid core was noted by S. Braginsky [*Geomagn. Aeron.* **4**, 572 (1964)].
16. The viscous stress-free boundary condition forces $\partial\omega/\partial r$ to vanish on the inner core boundary, so the net viscous torque Γ_ν vanishes there (*7*). This zero torque results in discontinuities in the horizontal velocity between the solid inner core surface and the fluid just above it, which make nonlinear contributions to the magnetic boundary conditions there.
17. F. D. Stacey, *Physics of the Earth* (Brookfield, Brisbane, Australia, ed. 3, 1992).
18. The computing resources were provided by the Pittsburgh Supercomputing Center under grant MCA94P016P and the Advanced Computing Laboratory at Los Alamos National Laboratory. Different aspects of this work were supported by Los Alamos Laboratory Directed Research and Development grant 96149, University of California Directed Research and Development grant 9636, Institute of Geophysics and Planetary Physics grant 713 and NASA grant NCCS5-147. P.H.R. was supported by NSF grant EAR94-06002. The work was conducted under the auspices of the U.S. Department of Energy, supported (in part) by the University of California, for the conduct of discretionary research by Los Alamos National Laboratory.

13 August 1996; accepted 29 October 1996

Tomography of the Source Area of the 1995 Kobe Earthquake: Evidence for Fluids at the Hypocenter?

Dapeng Zhao*, Hiroo Kanamori, Hiroaki Negishi, Douglas Wiens

Seismic tomography revealed a low seismic velocity (−5%) and high Poisson's ratio (+6%) anomaly covering about 300 square kilometers at the hypocenter of the 17 January 1995, magnitude 7.2, Kobe earthquake in Japan. This anomaly may be due to an overpressurized, fluid-filled, fractured rock matrix that contributed to the initiation of the Kobe earthquake.

The 17 January 1995, magnitude (*M*) 7.2, Kobe (Hyogo-Ken Nanbu) earthquake was the most damaging earthquake to strike Japan since the Kanto earthquake in 1923 (*1*). The Kobe earthquake occurred in an area with complex structure including numerous active Quaternary faults that have produced many large historical earthquakes (*2*). The permanent seismic networks in southwestern Japan (*3*) and many portable stations deployed following the Kobe mainshock (*4*) recorded thousands of aftershocks, which provide arrival time and waveform data for the determination of detailed crustal structure in the source area of the Kobe earthquake. Some previous tomographic studies found that some earthquake nucleation zones showed higher velocities than the surrounding country rock. These high velocity zones may represent competent parts of the fault zones or may indicate regions of transition from stable to unstable sliding (*5*). Other studies found that nucleation zones had low velocities and a high Poisson's ratio (σ) that suggested the existence of overpressurized fluids (*6, 7*). We conducted an investigation of the seismic structure in the Kobe earthquake source area to understand what may have triggered this earthquake and how the rupture proceeded after initiation.

We used the tomographic method of Zhao *et al.* (*8*) to determine the three-dimensional (3D) *P*- and *S*-wave velocity (V_p, V_s) and σ distribution maps in the source area of the Kobe earthquake. We used 3203 Kobe aftershocks and 431 local micro-earthquakes that generated 64,337 *P*- and 49,200 *S*-wave arrival times (Fig. 1). Most of the events were located in and around the rupture zone of the Kobe earthquake [the zone extends about 130 km northeast from the southern part of Awaji Island to Lake Biwa (Fig. 1)]. All the events were recorded by more than 15 stations, and the hypocenter locations are accurate to ±1 to 2 km (*4, 9*). The data were recorded by 37 permanent stations (*3*) and 30 portable stations that were set up following the Kobe mainshock (Fig. 1B) (*4*). The picking accuracy of *P*- and *S*-wave arrival times is 0.05 to 0.15 s (*3, 4*).

Large V_p and V_s variations of up to 6% and σ variations of up to 10% were revealed in the Kobe rupture zone (Figs. 2 to 4). The tomographic inversions imaged the Kobe rupture zone as a low velocity zone from the surface to a depth of 20 km with a width of 5 to 10 km (Figs. 3 and 4) (*10*). On average, V_p and V_s in the fault zone were 3 to 4% lower than the surrounding country rock velocities. V_p was slower in the northeastern segment of the aftershock zone (the Suma and Suwayama faults) than that in the southwestern segment (the Nojima fault on Awaji Island) (Fig. 2A), while V_s was slower along the Nojima fault (Fig. 2B). Therefore the Suma and Suwayama

D. Zhao and D. Wiens, Department of Earth and Planetary Sciences, Washington University, St. Louis, MO 63130, USA.
H. Kanamori, Seismological Laboratory 252-21, California Institute of Technology, Pasadena, CA 91125, USA.
H. Negishi, Disaster Prevention Research Institute, Kyoto University, Uji 611, Japan.

*To whom correspondence should be addressed. E-mail: dapeng@izu.wustl.edu